Observations of acyl peroxy nitrates during the front range air pollution and photochemistry éxperiment (FRAPPÉ)

Jake Zaragoza, Sara Callahan, Erin E. McDuffie, Jeffrey Kirkland, Patrick Brophy, Lindsi Durrett, Delphine K. Farmer, Yong Zhou, Barkley Sive, Frank Flocke, Gabriele Pfister, Christoph Knote, Alex Tevlin, Jennifer Murphy, Emily V. Fischer

RESEARCH ARTICLE

Correspondence to:
E. V. Fischer,
evf@atmos.colostate.edu

Observations of Acyl Peroxy Nitrates During the Front Range Air Pollution and Photochemistry Éxperiment (FRAPPÉ)

Jake Zaragoza[1,2], Sara Callahan[1,3], Erin E. McDuffie[4,5,6] (iD), Jeffrey Kirkland[7], Patrick Brophy[7,8] (iD), Lindsi Durrett[7], Delphine K. Farmer[7] (iD), Yong Zhou[1], Barkley Sive[9] (iD), Frank Flocke[10] (iD), Gabriele Pfister[10] (iD), Christoph Knote[11] (iD), Alex Tevlin[12] (iD), Jennifer Murphy[12] (iD), and Emily V. Fischer[1] (iD)

[1]Department of Atmospheric Science, Colorado State University, Fort Collins, CO, USA, [2]Now at Air Resource Specialists, Fort Collins, CO, USA, [3]Now at Department of Engineering, Smith College, Northampton, MA, USA, [4]Cooperative Institute for Research in Environmental Sciences, University of Colorado Boulder, Boulder, CO, USA, [5]Department of Chemistry, University of Colorado Boulder, Boulder, CO, USA, [6]Chemical Sciences Division, Earth System Research Laboratory, NOAA, Boulder, CO, USA, [7]Department of Chemistry, Colorado State University, Fort Collins, CO, USA, [8]Now at Proteomics and Metabolomics Facility, Colorado State University, Fort Collins, CO, USA, [9]Air Resources Division, National Park Service, Denver, CO, USA, [10]National Center for Atmospheric Research, Boulder, CO, USA, [11]Meteorological Institute, LMU Munich, Munich, Germany, [12]Department of Chemistry, University of Toronto, Toronto, ON, Canada

Abstract We report on measurements of acyl peroxy nitrates (APNs) obtained from two ground sites and the NSF/National Center for Atmospheric Research C-130 aircraft during the 2014 Front Range Air Pollution and Photochemistry Éxperiment (FRAPPÉ). The relative abundance of the APNs observed at the Boulder Atmospheric Observatory (BAO) indicates that anthropogenic emissions of volatile organic compounds (VOCs) are the dominant drivers of photochemistry during days with the most elevated peroxyacetyl nitrate (PAN). Reduced major axis regression between propionyl peroxynitrate (PPN) and PAN observed at BAO and from the C-130 produced a slope of 0.21 ($R^2 = 0.92$). Periods of lower PPN/PAN ratios (~0.10) were associated with cleaner background air characterized by lower ammonia and formic acid abundances. The abundance of methacryloyl peroxynitrate relative to PAN only exceeded 0.05 at BAO when PAN mixing ratios were <300 parts per trillion by volume, implying low influence of isoprene oxidation during periods with substantial local PAN production. We show an example of a day (19 July) where high O_3 was not accompanied by enhanced local PAN production. The contribution of biogenic VOCs to local O_3 production on the other days in July with elevated O_3 (22, 23, 28, and 29 July 2014) was small; evidence is provided in the high abundance of PPN to PAN (slopes between 0.18 and 0.26). The PAN chemistry observed from surface and aircraft platforms during FRAPPÉ implies that anthropogenic VOCs played a dominant role in PAN production during periods with the most O_3 and that the relative importance of biogenic hydrocarbon chemistry decreased with increasing O_3 production during FRAPPÉ.

1. Introduction

Approximately 80% of the population of Colorado lives in the Northern Front Range Metropolitan Area (NFRMA), encompassing the cities of Denver, Boulder, Longmont, Greeley, and Fort Collins. The NFRMA is currently an ozone (O_3) nonattainment area (Cooper et al., 2015), and this region is expected to remain out of compliance with a more stringent National Ambient Air Quality Standard (NAAQS) for O_3. Unlike the metropolitan regions located in the eastern U.S., where summertime O_3 abundances have sharply declined over the last two decades (Cooper et al., 2014; Simon et al., 2015), summertime O_3 in the NRFMA has increased (Strode et al., 2015). There is evidence that the most recent period of increase (2009–2013) is the result of increases in O_3 precursor emissions in the region (Reddy & Pfister, 2016).

The NFRMA is characterized by urban sources of O_3 precursors that abut regions with large emissions from oil and natural gas production. The NFRMA has experienced relatively rapid population growth, between 4 and 11% over the most recent 5 year period depending on the county (www.census.gov/). Emissions from fossil fuel extraction in the NFRMA are poorly constrained (Gilman et al., 2013; Pétron et al., 2012; Swarthout et al., 2013; Thompson et al., 2014) but make a major contribution (~50%) to the VOC-OH reactivity (a measure of the relative contribution of VOCs to the potential to form O_3) in the region throughout the year (Abeleira et al., 2017; Gilman et al., 2013; McDuffie et al., 2016; Swarthout et al., 2013). The region lacks consistent

long-term in situ observations of NO_x needed for a thorough examination of trends in this precursor throughout the region, but satellite (Strode et al., 2015) and existing surface measurements (Abeleira & Farmer, 2017) provide evidence of decreases in NO_x abundances between 2000 and 2015. The percent decrease in NO_x inferred from satellite observations of NO_2 columns is similar to that observed over the eastern U.S., but the absolute decrease is smaller (Strode et al., 2015).

Acyl peroxy nitrates (APNs) are secondary species often formed alongside O_3 in polluted air masses (Singh & Hanst, 1981). The chemistry of APNs is partially responsible for the positive relationship observed between O_3 and temperature; the formation of APNs represents an increased sink of NO_x and odd hydrogen as temperatures decrease (Sillman & Samson, 1995). When elevated abundances are present, APNs act as respiratory irritants and lachrymators (Vyskocil et al., 1998); they also damage vegetation (Taylor, 1969). APNs can constitute a significant portion of the reactive nitrogen oxide budget (NO_y), particularly in remote regions, where they are often more abundant than NO_x (Roberts et al., 2004; Singh, 1987; Singh et al., 1985, 1994). PAN ($CH_3C(O)O_2NO_2$) is the most abundant member of the APN family. Both biogenic and anthropogenic VOCs can contribute to PAN formation (Fischer et al., 2014). Other abundant members of the APN family include methacryloyl peroxynitrate (MPAN; $CH_2C(CH_3)C(O)OONO_2$) and propionyl peroxynitrate (PPN; $CH_3CH_2C(O)OONO_2$), and their formation has been attributed to particular emitted precursors or oxidation intermediates. The relative abundance of these two different APN homologues have been used to diagnose which VOCs are photochemically important in a region (Roberts et al., 1998, 2003; Williams et al., 1997).

During July and August 2014, ground-based and airborne measurements of O_3 precursors and aerosols were conducted as part of the Front Range Air Pollution and Photochemistry Éxperiment (FRAPPÉ) field intensive (Dingle et al., 2016; McDuffie et al., 2016; Vu et al., 2016). The campaign was simultaneous with the final phase of the NASA Deriving Information on Surface conditions from Column and Vertically Resolved Observations Relevant to Air Quality mission (http://discover-aq.larc.nasa.gov/). In this study, we present measurements of the APNs and relevant supporting data from the C-130 and two ground sites: the Boulder Atmospheric Observatory (BAO) and a location on the edge of Rocky Mountain National Park (RMNP). We focus on the analysis of the data from BAO because measurements of multiple APNs were made at this location, and there are other manuscripts in development that will investigate the RMNP data set.

2. Methods

2.1. Site Descriptions

The Boulder Atmospheric Observatory (BAO) (40°N, 105°W, 1,584 m above sea level (asl)) was one of the ground-based sites that housed a large suite of trace gas and aerosol measurements during FRAPPÉ (Figure 1). Recent winter (2011) (Gilman et al., 2013; Swarthout et al., 2013), spring (2015) (Abeleira et al., 2017), summer (2012 and 2015) (Abeleira et al., 2017; McDuffie et al., 2016), and multiyear (2007–2010) (Pétron et al., 2012) measurements from BAO have investigated the sources and impacts of VOC emissions on trace gas composition in the NFRMA. Though VOCs have been characterized at BAO during past campaigns, this type of data was not available in 2014.

BAO had a 300 m tower outfitted with a suite of meteorological instrumentation, including wind speed and direction, at three different levels (10, 100, and 300 m above ground level) (Hahn, 1981; Kaimal & Gaynor, 1983). During FRAPPÉ, instruments were housed in either a vertically mobile carriage mounted on the south-southwest face of the BAO tower (Brown et al., 2013), or a trailer parked at the base of the tower. The PAN instrument was located in the trailer at the base of the tower. The carriage, known as the Profiling Instrument Shelter with Amenities (PISA), was used for both vertical profiling and stationary measurements (McDuffie et al., 2016). For FRAPPÉ, the PISA sheltered several instruments described further in section 2.3. PAN measurements were made at BAO between 9 July and 22 August 2014, the start and end dates for the other supporting measurements varied.

We also present data collected near the edge of Rocky Mountain National Park (40.3°N, 105.5°W, 2,743 m asl). The site is located on the east side of the Continental Divide and co-located with the Interagency Monitoring of Protected Visual Environments and Environmental Protection Agency (EPA) Clean Air Status and Trends Network monitoring sites. There is a history of observations of atmospheric reactive nitrogen species at
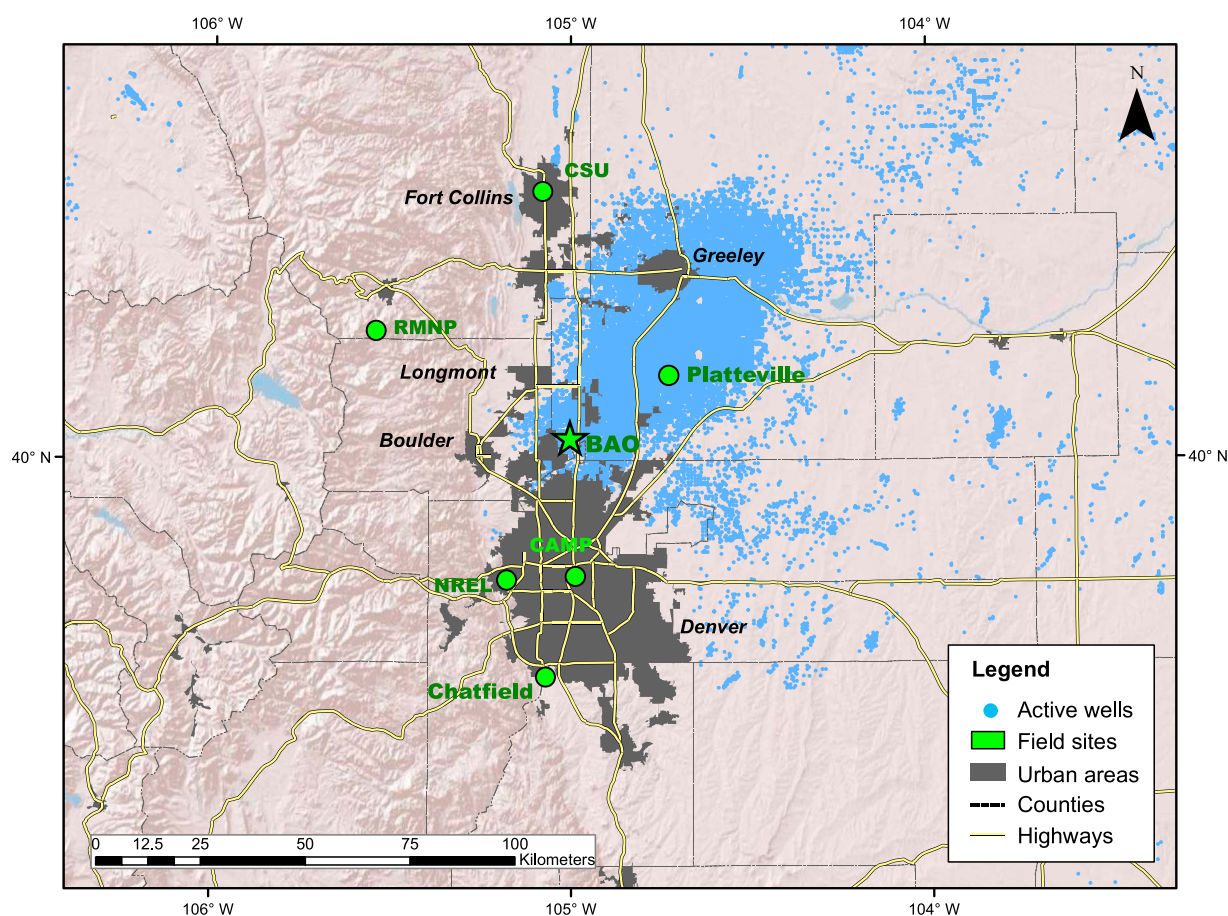
Figure 1. Map of region with the location of major FRAPPÉ sites (green), oil and gas wells (blue), highways (yellow), and major urban areas (grey).

this location (e.g., Benedict et al., 2013), but to our knowledge, we present the first measurements of PAN at this location. PAN measurements were made at RMNP between 11 July and 31 August 2014.

2.2. APN Measurements

PANs at BAO were measured with the National Center for Atmospheric Research (NCAR) gas chromatograph with an electron capture detector (NCAR GC-ECD) (Flocke et al., 2005). The NCAR PAN GC-ECD is a dual-channel system with a common sampling loop and ECD. A full description of the instrument can be found in Flocke et al. (2005). For this campaign, the NCAR GC-ECD was configured to collect a point sample every 5 min. The sampling inlet was located at a height of ~6 m on scaffolding erected above the trailer. PAN was sampled through a 0.476 cm internal diameter Teflon line with a 1 μm Teflon filter located at the inlet. Flow through the 7.3 m line was approximately 7 liters per minute (Lpm), yielding a residence time of less than a second in the main inlet. Under the afternoon conditions typical of BAO during FRAPPÉ, the lifetime of PAN is ~2 h; thus, we do not expect significant decomposition in the inlet. The instrument subsampled off this main line at a slower flow rate (~50 mL/min). PAN spent under 3 min in the instrument. At 20°C PAN has a lifetime against thermal dissociation of ~85 min, which yields a potential thermal loss of <5% from thermal dissociation within the instrument; however, our calibration procedure also corrects for this.

Automated single-point calibrations were performed throughout the campaign at 4 h intervals, with more frequent calibrations during the initial week of the campaign. Point calibrations were augmented by multi-point calibration midcampaign. The PAN standard was generated using a continuous-flow acetone photolysis cell (Volz-Thomas et al., 2002; Warneck & Zerbach, 1992). Briefly, peroxyacetyl radicals were generated by the 285 nm photolysis (Jelight Part Number: 84–285-2) of 20 ppmv acetone in ultrazero air (Scott-Marrin Tank Number: CB10757) in the presence of O_2. An accurately measured flow of NO (1 ppmv NO in N_2, Scott-Marrin

Tank Number: CB10671) was added to the gas stream. A zero air generator was used as a dilution source. To calculate our final PAN mixing ratios, we assumed a calibrator efficiency of 93% for the conversion of NO to PAN. MPAN and PPN were not directly calibrated. Instead, their mixing ratios were obtained using the response factors relative to PAN (0.90 ± 0.02 and 0.64 ± 0.03, respectively) in Flocke et al. (2005). Flocke et al. (2005) determined these relative responses using sources of the individual compounds.

The calibrator uncertainty was determined to be 8% via a root sum of squares calculation of the uncertainty of the calibration gases (2% for NO), gas flow controllers (1% for acetone, 3% for NO, and 6% for the zero air generator), and the calibrator efficiency (3%). Acetone is present in excess, so the 5% stated uncertainty on the standard mixing ratio is irrelevant. Beginning in the last week of July and extending through the end of the campaign, some of the chromatogram baselines sporadically became noisy as a result of an unknown electrical interference. This resulted in separate precision and limit of detection calculations for "clean" and "noisy" baselines. The precision of the campaign-wide point calibrations was determined by calculating the relative standard deviation of PAN peak areas in both columns, for the clean and noisy baselines, resulting in four different precision calculations (6% and 4% for PAN on columns 1 and 2, respectively, for clean baselines and 3% for PAN on both columns for noisy baselines). The uncertainty was calculated as the root sum of squares of the uncertainty of the calibrator and precision of the point calibrations, resulting in four different uncertainties (11 and 10% for PAN in columns 1 and 2, respectively, for clean baselines and 10% for PAN on both columns for noisy baselines). The precision and uncertainty values on the noisy baselines are lower because we increased the sample pressure in an effort to increase peak size. The limits of detection (LOD) were calculated as three times the standard deviation of the baseline during example clean and noisy periods. The LODs were approximately 2 parts per trillion by volume (pptv) for clean chromatograms and 20 pptv for noisy chromatograms. As a result of the electrical noise, we only quantified MPAN during July.

PAN was measured at RMNP with a custom gas chromatograph using a ThermQuest ECD held at 50°C. The instrument was configured to only separate and quantify PAN, not its homologues. The output voltage from the electrometer was converted to a digital signal by Shimadzu Software (Version 7.4 SP2); this software was used to control the valve position and to perform the peak integrations off-line. We used a similar Teflon inlet and filter at RMNP to that described above for BAO. At RMNP the sampling inlet for the PAN GC was located 8.5 m above ground level, with a total inlet length of 13.4 m. Flow through the line was approximately 10 Lpm. The instrument sampled off this main line at a slower flow rate (~35 mL/min). A 1.5 mL sample was injected every 5 min onto a precolumn using a 10-port Valco sampling valve. The sample loop was made from 0.32 cmpolyetheretherketone (PEEK) tubing and the connecting tubing material from the sampling valve to the column was 0.16 cm PEEK. Ultrahigh purity (UHP) helium (He) was used as a carrier gas, and UHP nitrogen (N_2) was used as a makeup gas. The carrier and makeup gases were both further purified with a Valco Helium Purifier (HP2) and a Supelpure-O (22449) trap, respectively. The carrier gas flow was ~25 mL/min, and the makeup gas flow was ~3–4 mL/min. Similar to Flocke et al. (2005), we humidified the carrier gas by flowing it through a cartridge filled with copper(II) sulfate pentahydrate, temperature controlled to 35°C. We used two ~6 m sections of Restek Rtx-200 (1 μm film thickness, 0.53 mm ID) capillary column as precolumn and main column. The 10-port valve, the columns, the connecting tubing, and needle valves were situated in an insulated box controlled to 18°C using a bidirectional temperature controller (TE Technology TC 36-25 RS232) and a thermoelectric device (TE Technology AC-073). We set our back flush of the precolumn to occur at 1.9 min. This combination of temperature, flow rates, and valve switch time yielded a PAN retention time of approximately 2.8 min. We estimate that PAN spent approximately 3 min in the instrument.

We performed manual calibrations at RMNP weekly, and often bi-weekly, throughout the campaign. As at BAO, PAN was generated using an acetone photolysis cell with accurately measured flows of acetone in UHP zero air (20 ppbv acetone) and 1 ppm NO in nitrogen (Scott-Marrin Cylinder Numbers: CB09819 and CB11156). We used an Airgas cylinder of UHP zero air to dilute the output of the calibrator rather than a zero air generator. Again, the calibrator efficiency was assumed to be 93% for the conversion of NO to PAN (Volz-Thomas et al., 2002). The uncertainty of the RMNP calibrator was determined to be 6% via a root sum of squares calculation of the uncertainty of the calibration gases (2% for NO), laboratory tests of the gas flow controllers (1% for acetone, 1% for NO, and 1% for the zero air generator), and the calibrator efficiency (3%). The precision of the system was estimated as 4% in a laboratory setting and 6% by repeatedly sampling a constant source of PAN over the weekly calibrations between 25 July and 8 September. Prior to 25 July, the weekly calibrations indicate a lower system precision (9%), due to a problem with the inlet pressure

control. On the basis of chromatograms collected during the most pristine periods at RMNP, we estimate an on-site detection limit of ~10 pptv.

2.3. Supporting Measurements at BAO

Measurements of CO, CO_2, and CH_4 were made using a four-channel Picarro Cavity Ring-Down Spectrometer (CRDS, Picarro Model G2401). During FRAPPÉ, a short inlet (~1 m) associated with the Picarro was located on the bottom of the carriage, and air was sampled through an in-line 7 μm filter. Five NOAA standard reference gases (http://www.esrl.noaa.gov/gmd/ccl/refgas.html) were used for calibrations. Two standard reference gas mixtures (JA02336 and JB03049) were used as field calibration standards during the campaign at 3 h intervals, and three standard reference gas mixtures (CA06969, CB10166, and CA08244) were used to perform laboratory instrument calibrations, precampaign and postcampaign. Mixing ratios were calculated using these scales: WMO-CH4-X2004 and WMO-CO-X2014. We estimate the uncertainty associated with the CH_4 and CO data to be 6% and 12%, respectively. Uncertainty was approximated as the quadrature sum of measurement precision, calibration uncertainty and uncertainty in the water vapor correction. NO_x, NO_2, O_3, and NO_y were measured from the PISA with a custom-built, multichannel cavity ring-down instrument as described in detail by McDuffie et al. (2016, and references therein) with accuracies of <5% for NO_x, NO_2, and O_3 and <12% for NO_y. O_3 was also measured from an inlet attached to the ground-based trailer housing the NCAR PAN-GC with a 2B Technologies Model 202 Ozone Monitor. The 0.635 cm OD (1/4″ OD) Teflon inlet was located at a height of 5.08 m and pulled through ~6 m of tubing at approximately 1 Lpm. The Model 202 was calibrated before, once during, and after the campaign with a 2B Technologies Model 306 Ozone Calibration source.

Ammonia mixing ratios were measured from the PISA using a quantum cascade tunable infrared laser differential absorption spectrometer instrument (Aerodyne Research Inc.). Air was sampled at approximately 10 Lpm through 3 m of PFA tubing, using an inertial inlet mounted on the outer wall of the carriage in order to remove particles without the use of a filter (Ellis et al., 2010). Calibrations were carried out approximately every 72 h by introducing a constant mixing ratio of 1.7 ppbv NH_3 from a permeation source (KIN-TEK Laboratories, Inc.), and spectral baselines were determined every half hour by sampling NH_3-free air generated using a palladium catalyst heated to 360°C (Aadco Instruments).

Formic acid was measured on the PISA platform with a high-resolution time-of-flight chemical ionization mass spectrometer (CIMS) (Aerodyne Research Inc.; $m/\Delta m \sim 4{,}000$) implementing acetate ion chemistry. The inlet was ~1 m of 0.635 cm OD PEEK tubing. Background count rates and sensitivities to formic acid were determined by hourly calibrations with a formic acid permeation tube (KinTek) diluted by UHP zero air (Mattheson) using both external standard and standard addition approaches (Brophy & Farmer, 2015). Detection limits for formic acid are typically <100 pptv.

2.4. Supporting Measurements at RMNP

There were a number of supporting measurements made at RMNP during the FRAPPÉ period including other gas phase reactive nitrogen species (NO, NO_2, NO_x, NO_y and NH_3, and select alkyl nitrates), a suite of VOCs, and O_3. The methods associated with these measurements are the topic of a forthcoming manuscript.

2.5. Description of FLEXPART Model

FLEXPART is a Lagrangian particle dispersion model used to simulate atmospheric transport and dispersion (Stohl et al., 2005). For this application, a version of FLEXPART was used that was coupled to the Weather Research and Forecasting (WRF) model (http://www.wrf-model.org) as described by Brioude et al. (2013). WRF was set up using a 15 km resolution domain over the western U.S. with an inner domain at 3 km horizontal resolution over the domain of Colorado and adjacent states. For FRAPPÉ, FLEXPART was run forward in time to understand the dispersion of different emissions sources and backward to understand the history of air parcels impacting specific sites. The model was run for BAO but not for RMNP as part of FRAPPÉ. In the case of the "backward" runs, 100,000 particles—representing inert air tracers—were released during the first hour at each release point (e.g., BAO) randomly between 0 and 100 m above ground level, and followed backward in time for 24 h. At each hour, the spatial distribution of particles in the lowest 100 m was multiplied with a gridded description of emission fluxes from various sources.
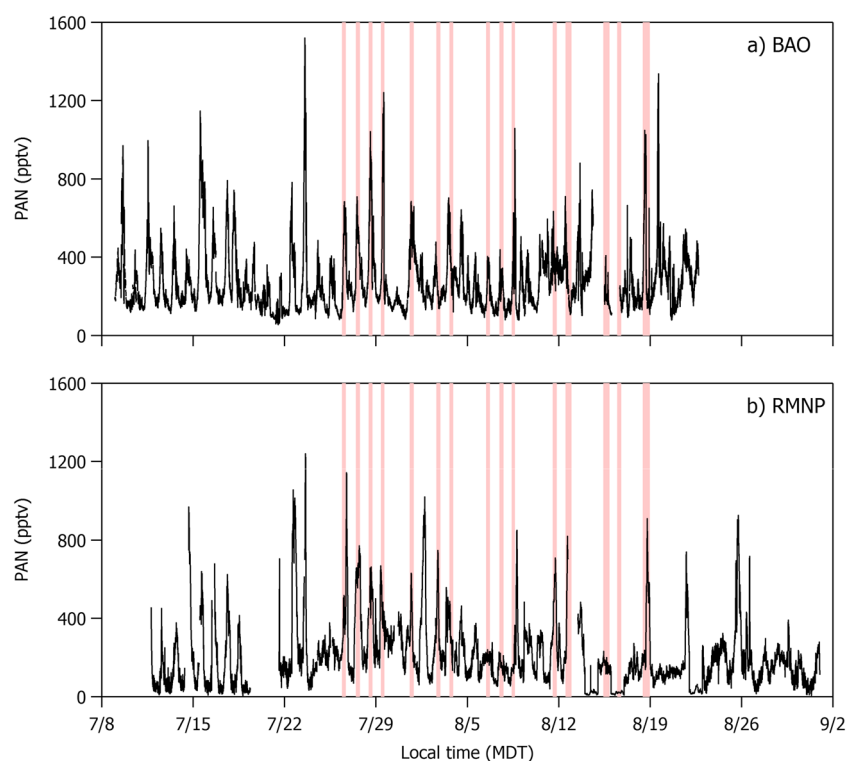
Figure 2. Time series of PAN mixing ratios. The reddish bars signify C-130 flight days.

Fire emissions within the FLEXPART modeling framework used here were based on the Fire Inventory from NCAR (Wiedinmyer et al., 2011). Emissions of isoprene and lumped monoterpenes were based on the Model of Emissions of Gases and Aerosols from Nature (MEGAN) (Guenther et al., 2006). Agricultural emissions (NH_3) were based on the 2011 EPA National Emission Inventory (NEI). Area and Mobile sources are from a Colorado Department of Public Health and Environment emission inventory projected for 2018. Emissions of ethane (a proxy for oil and gas activities) were from the Western Regional Air Partnership (https://www.wrapair2.org/PhaseIII.aspx) 2008 inventory.

3. Results and Discussion

3.1. Overview of Chemical Measurements

Figure 2 presents a time series of the 5 min PAN data for BAO and RMNP for the FRAPPÉ campaign. Similar to observations at other ground sites (Grosjean et al., 2001; Ridley et al., 1990; Roberts et al., 1998, 2003), PAN shows a pronounced diurnal cycle at both locations, reflecting daytime photochemical production and nighttime deposition. At BAO, daytime hourly PAN was positively correlated with NO_z (NO_y-NO_x) throughout the campaign, with a median PAN/NO_z ratio of 0.13.

Table 1 presents mean, median, and maximum PAN, PPN, and MPAN mixing ratios for the entire campaign. The maximum PAN mixing ratio for each site was observed on 23 July. Table 1 also provides summary statistics for the aircraft PAN observations collected during the FRAPPÉ campaign. PAN was measured on the C-130 research aircraft with a thermal dissociation chemical ionization mass spectrometer (CIMS) (Zheng et al., 2011). For comparison with the BAO and RMNP PAN data, we confined data from the C-130 to approximately 40–41°N and 104–105°W below 3 km. In general, the C-130 average is expected to be higher because C-130 flights were made during the day, usually in the afternoon, when photochemistry is most active. Only one out of the four days with the highest afternoon PAN mixing ratios observed at BAO had a concurrent C-130 research flight (red shading in Figure 2).

Dingle et al. (2016) point out the regional influence of biomass burning in the Front Range between 11 and 12 August. The presence of smoke increased the background aerosol optical extinction by 10–15 Mm^{-1}.

Table 1

Mean, Median, and Maximum (With Corresponding Day) 5 min Point Mixing Ratios for PAN, PPN, and MPAN at BAO (1 min Average Mixing Ratios) on the C-130 (40–41°N and 104–105°W Below 3 km) and 5 min Point Mixing Ratios at RMNP During FRAPPÉ

	PAN (pptv)			PPN (pptv)			MPAN (pptv)		
	Mean	Median	Max	Mean	Median	Max	Mean	Median	Max
BAO	275	223	1519 (23 July)	38	26	307 (23 July)	9	7	36 (29 July)
C-130	667	613	1975 (28 July)	106	88	393 (28 July)	NA	NA	NA
RMNP	201	163	1327 (23 July)	NA	NA	NA	NA	NA	NA

Note. As a result of the noisy baselines in August on the NCAR PAN GC, MPAN mixing ratios were only quantified for July. Below detection limit measurements were included in the statistics as one half the detection limit. NA, not available.

During this time period, afternoon PAN maxima at both sites varied between 600 and 700 pptv, and there was a change in the diurnal cycle of PAN at BAO. Specifically, nighttime PAN mixing ratios remained largely above 300 pptv, in contrast to the rest of the campaign, where overnight mixing ratios typically dropped to ~150 pptv. We did not observe a different relationship between PPN and PAN during this time period compared to the rest of the campaign (see section 3.3).

3.2. Regional Mixing During FRAPPÉ: Examples From Elevated PAN Periods

McDuffie et al. (2016) showed that BAO was influenced by regional emission sources from several sectors regardless of the local wind direction during the FRAPPÉ period. We use the four days (15, 23, and 29 July and 19 August) at BAO with the highest PAN mixing ratios (PAN >1 ppbv) to demonstrate that using wind direction alone provides limited information on upwind sources. All the FLEXPART air parcel histories presented in Figure 3 suggest mixing of various emission sectors during the days with the most elevated PAN at BAO. The air parcel loading plot for 15 July (Figure 3a) indicates that agricultural emissions impacted the air parcel 3–9 h before it arrived at BAO, and emissions from oil and gas activities impacted the air parcel during the 8 h prior to arrival at BAO. This day (15 July) is noteworthy because National Weather Service (NWS) surface winds show strong upslope (easterly) flow at the surface in the morning (07:00–09:00 a.m. MT), sweeping emissions (largely from oil and gas operations) from east toward the urban Front Range. In Figures 3b and 3c (23 and 29 July respectively) air parcel histories both show various emission source sectors (i.e., biogenic, mobile sources, oil and gas operations, and other area/point sources) mixing over the Front Range en-route to BAO. NWS stations also show easterly winds throughout the morning of 23 July, sweeping emissions from the east into urban regions. In summary, the air parcels with the highest PAN observed at BAO during FRAPPÉ likely contain emissions from multiple sources throughout the region. We also found this to be true of periods without elevated PAN, and the results of this analysis are presented in Zaragoza (2016).

Figure 3 shows that when elevated PAN was observed the air often traveled over the Denver-Julesburg Basin, located to the northeast of BAO, before arriving at the BAO site, and we did observe a positive relationship between hourly afternoon averaged PAN and CH_4. Methane is not a precursor for PAN, but larger coemitted alkanes from oil and gas activities can contribute to PAN formation. As discussed in Pétron et al. (2014), there are other sources of CH_4 located to the northeast of BAO in addition to oil and gas activities. Beef production and dairy production are major activities in Weld County located to the northwest of BAO, and there are also landfills and wastewater treatment facilities that contribute to CH_4 and VOC emissions. Based on measurements in 2012, Pétron et al. (2014) estimated that 75% of the total CH_4 emissions in this region could be attributed to oil and gas activities. Based on isotopic measurements during the 2014 FRAPPÉ period, Townsend-Small et al. (2016) estimated that at least 50% of the CH_4 emissions in this region were from biogenic sources. Other more specific VOC tracers of oil and gas activities, e.g., ethane, were not measured at BAO during FRAPPÉ. In summary, while we do not know the temporal (or even average) contribution of emissions from oil and gas activities to air parcel composition at BAO during FRAPPE, it is expected to have been substantial.

3.3. PAN, PPN, and MPAN Relationships at BAO

The ratio of PPN/PAN has been used previously to indicate the relative importance of PAN precursor species. A PPN to PAN ratio of ~0.15 has been observed in a number of urban areas (e.g., Roberts et al., 1998, 2002, 2003)
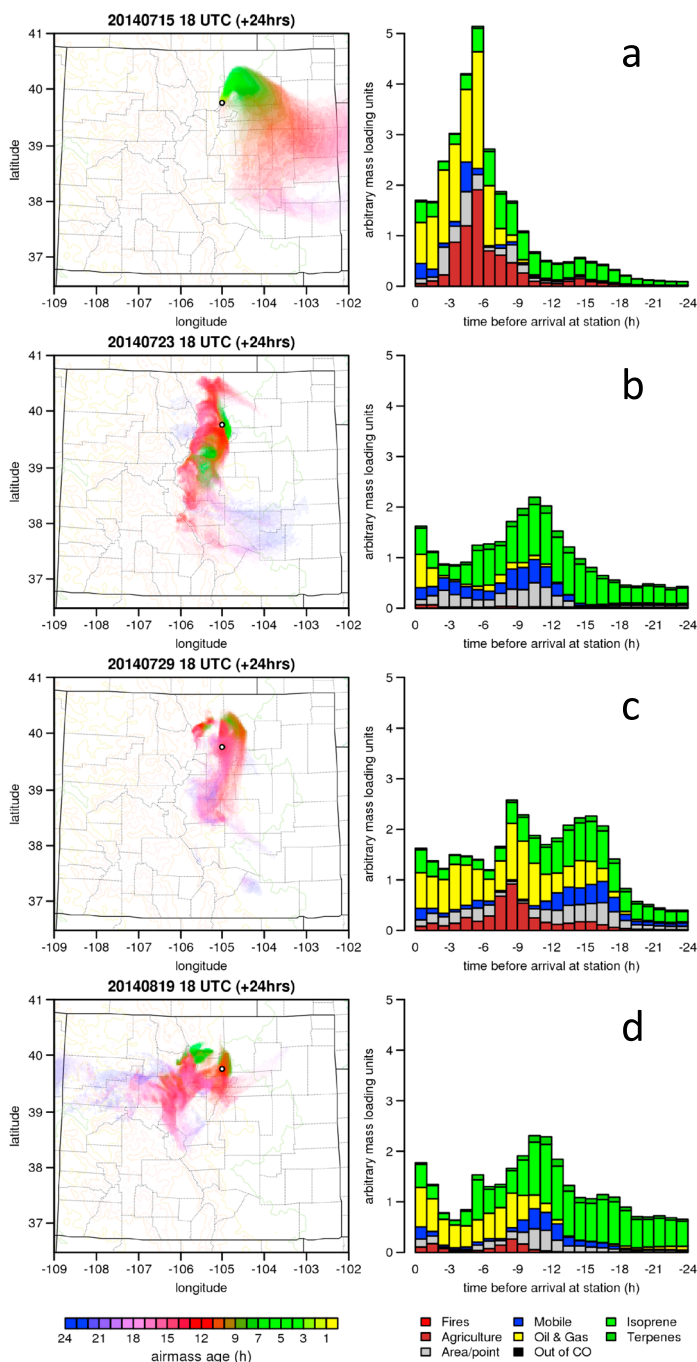
Figure 3. FLEXPART output for (a) 15, (b) 23, and (c) 29 July and (d) 19 August 2014. (left) The 24 h air mass histories for air impacting BAO between 11 a.m. and 12 p.m. MT. The circle represents the location of the BAO tower. These maps show the spatial distribution of particles used to calculate the stacked bars to the right, color-coded by the hours since release. (right) The contribution (over time) of various emission sources to the air parcel observed at BAO. At each hour shown these graphs, the spatial distribution of particles in the lowest 100 m was multiplied with a gridded description of emission fluxes from various sources. The sum over all grid cells of the result for each source category is plotted as stacked bars. Thus, the stacked bars represent the contribution (over time) of each emission source, in arbitrary mass units, to the air measured at the release point during the time the particles were released. All source categories decayed at the same e-folding lifetime of 48 h and the stacked bars have been scaled accordingly. The order of the stacked bars corresponds to the legend from left to right and top to bottom; i.e., the bottom bar is associated with fires and the top bar is associated with terpenes.
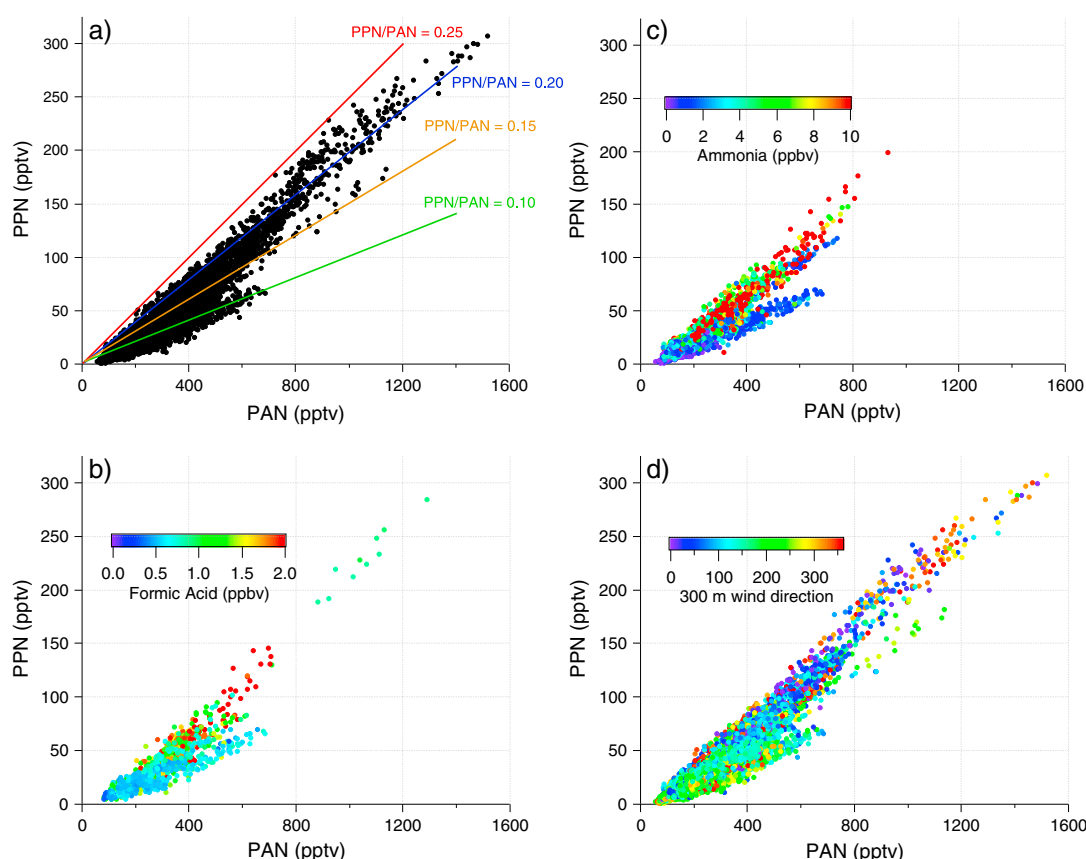
Figure 4. (a) Simultaneous 5 min point PPN versus PAN observations from BAO for the FRAPPÉ entire campaign. The colored lines denote potential ratios of PPN to PAN and are not linear fits to the data. (b) The 5 min point PPN versus PAN observations from BAO colored by simultaneously observed ammonia mixing ratio where available. (c) The 5 min point PPN versus PAN observations from BAO colored by simultaneous observed formic acid mixing ratio where available. (d) The 5 min point PPN versus PAN observations from BAO colored by 300 m wind direction. Similar patterns are present in the 100 and 10 m wind observations.

and has been shown to reflect PAN production from a mixture of anthropogenic VOCs, primarily from mobile sources. PAN can also be formed from VOC mixtures dominated by isoprene or its oxidation products, but PPN is not. The main intermediate precursor for PPN is propanal (Roberts et al., 2001, 2007). The fractional abundance of MPAN relative to PAN has been used to indicate the importance of biogenic VOCs in PAN (and O_3) production (Williams et al., 1997). Methacrolein is a first-generation product of isoprene oxidation, and this is thought to be the only significant precursor for MPAN.

The relationship between PPN and PAN at BAO during FRAPPÉ is shown in Figure 4a. The slope of the entire data set, determined by reduced major axis (RMA) regression, was 0.21 ($R^2 = 0.92$). The colored lines on Figure 4a indicate relative abundances of PPN to PAN ranging from 0.10 to 0.25. Periods with the most elevated PAN mixing ratios presented PPN/PAN ratios >0.15. The most elevated PAN periods corresponded to PPN/PAN ratios >0.20.

Periods of time with PPN/PAN ratios near 0.10 appear to be associated with relatively cleaner background air. These lower PPN/PAN ratio periods were characterized by lower NH_3 and formic acid (Figures 4b and 4c). NH_3 and formic acid were only trace gas measurements during the BAO field campaign that clearly showed different abundances associated with different PPN/PAN ratios, and that is why they are plotted in Figure 4. The NH_3 and formic acid measurements were both made from the PISA tower from varying altitudes and over shorter time periods than PAN, 30 July to 20 August and 18 July to 8 August, respectively. Formic acid is produced during the oxidation of VOCs, and it can also be emitted directly (Millet et al., 2015). Formic acid mixing ratios were consistently low (<0.75 ppbv) during periods with PPN/PAN ratios near 0.10. Tevlin et al. (2017) show that the highest mixing ratios of NH_3 were observed under periods
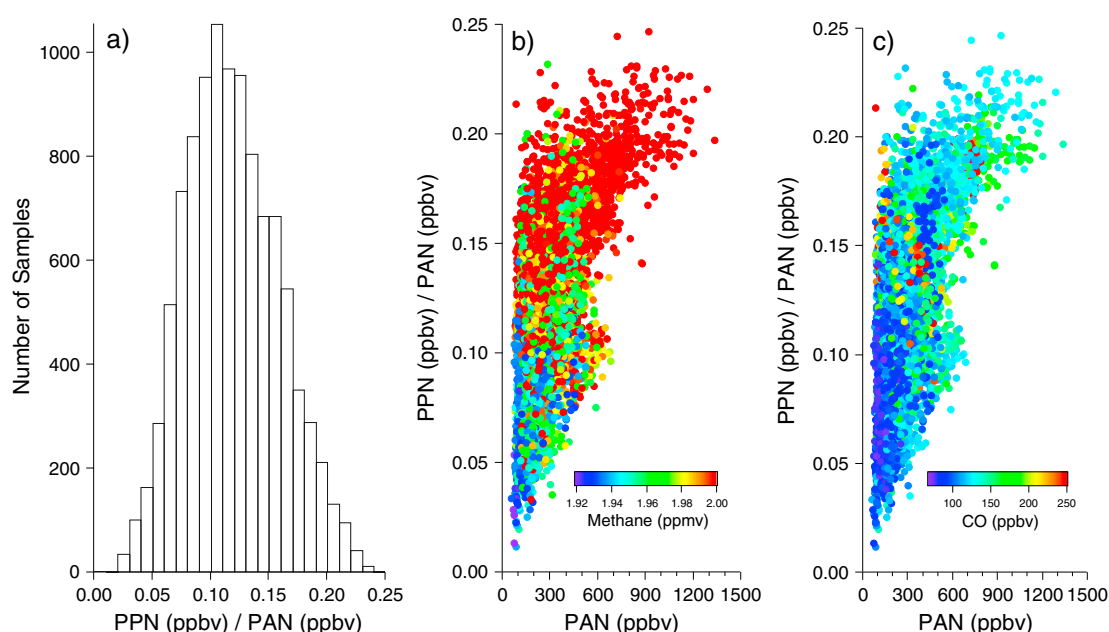
Figure 5. (a) Histogram of PPN to PAN ratios in 5 min point samples at BAO. (b) PPN to PAN ratio in 5 min point samples versus the coincident PAN mixing ratio colored by the coincident CH_4 mixing ratio. (c) PPN to PAN ratio in 5 min point samples versus the coincident PAN mixing ratio colored by the coincident CO mixing ratio.

of northeasterly flow: the direction where major concentrated animal feeding operations and oil and gas development are located. They also show that the lowest mixing ratios were observed under periods of westerly and southwesterly flow.

Figure 4d presents the same data in Figure 4a colored by 300 m wind direction. The PPN/PAN ratio observed at BAO does not cleanly split by wind direction based on any altitude of measurement; however, Figure 4d does indicate that low PPN/PAN ratios are most commonly associated with winds with a southerly component (90°–270°). Higher PPN/PAN ratios are more commonly associated with winds with a northerly component (270°–90°). There is more oil and gas development to the north of the site than to the south (Figure 1). There is also a weak time of day dependence (not shown); lower PPN/PAN ratios are more common in the evening and after sunset (17–23 MT). Removing data with low wind speeds does not improve the ability of wind direction to predict PPN/PAN relationships.

Figure 5a presents a histogram of PPN/PAN ratios for individual measurements. Taken together with Figure 4a, this shows that the RMA slope of 0.21 for PPN versus PAN is heavily weighted by the highest PAN and PPN mixing ratios. In other words, the highest PAN mixing ratios are consistently associated with high PPN/PAN ratios and appear to reflect relatively little variability in VOC chemistry between different high PAN days (discussed more below). Figures 5b and 5c show that the lowest PAN mixing ratios and low PPN/PAN ratios were often associated with near background abundances of CH_4 and CO. Although peak values up to 7 ppmv and 500 ppbv for CH_4 and CO, respectively, were observed, the scales in Figures 5b and 5c are truncated to highlight the lower end of the distribution; 2 ppmv represents the 55th percentile of the distribution for CH_4, and 250 ppbv represents the 99th percentile of the distribution for CO. The NCAR C-130 data were confined to the same area and height as mentioned in section 3.1, and the PPN/PAN ratio in this subset of data was also found to be 0.21(via RMA). A similar ratio (0.21) was also observed in wintertime PANs data obtained from the Uintah Basin in Utah (Patrick Veres, personal communication), a rural region with substantial oil and gas production that contribute to emissions of alkanes (e.g., Helmig et al., 2014; Warneke et al., 2014). Thus, we hypothesize that this ratio is indicative of a large PAN source from the oxidation of alkanes from oil and gas production.

PAN can be formed from many different VOC precursors with varying yields (Fischer et al., 2014). The high abundance of alkanes in the Colorado Front Range distinguishes the VOC composition in this region from

other U.S. cities (Abeleira et al., 2017). There are several possible ways that this type of VOC mixture could produce more PPN relative to PAN than other regions. For example, propanal and thus PPN formation would be expected from the formation and subsequent thermal decomposition of alkoxy radicals from butane and pentane oxidation. Elevated propane in the region could also hypothetically contribute to the high PPN/PAN ratio. Propanal is always the immediate precursor for PPN. The reaction between propane and OH only forms propanal with a 28% yield (Atkinson et al., 1985; Droege & Tully, 1986), but both Gilman et al. (2013) and Abeleira et al. (2017) showed that the mean propane mixing ratios at BAO are much greater than other U.S. cities.

For comparison, Ridley et al. (1990) measured PAN species at Niwot Ridge, approximately 30 km west of Boulder at 3,050 m asl from 16 June to 31 July 1987, and at the NCAR Mesa Lab near Boulder from 30 May to 10 June and from 11 August to 24 September 1987. These data indicate that PPN/PAN ratios in 1987 at these locations were dependent on wind direction and ranged from 0.04 when winds were westerly, coming from the remote mountains of Colorado, to 0.15 when winds were easterly, indicative of impact from the urban Colorado Front Range. The highest daytime PPN/PAN ratios measured at BAO during FRAPPÉ were mainly associated with winds with a northerly component (270°–90°). The ratios observed during summer 2015 were also greater than those measured by Ridley et al. (1990).

MPAN is formed during isoprene oxidation via the oxidation intermediate methacrolein (Bertman & Roberts, 1991; Nouaime et al., 1998; Tuazon & Atkinson, 1990; Williams et al., 1997). The MPAN/PAN ratio during July 2014 at BAO was consistently less than 0.10, but MPAN/PAN ratios only exceeded 0.05 when PAN mixing ratios were less than 300 pptv. PAN mixing ratios above 600 pptv were associated with MPAN/PAN ratios between 0.02 and 0.03, suggesting very little influence of local isoprene chemistry on APN formation compared to published data sets from other regions (Roberts et al., 1998, 2003, 2007). There is evidence that vehicle exhaust can also be a direct source of both isoprene and methacrolein (Biesenthal & Shepson, 1997; Jonsson et al., 1985; McLaren et al., 1996; Schauer et al., 2002). Based on the calculations in Zaragoza (2016), we do not think that vehicle exhaust is the dominant source of isoprene in the NFRMA. Zaragoza (2016) compared anthropogenic emissions of isoprene and methacrolein from the 2011 NEI and daytime biogenic isoprene emissions from MEGAN. The fraction of MPAN from anthropogenic emissions was calculated assuming a 25% yield of methacrolein from isoprene, based on isoprene oxidation under high NO_x conditions, and a 50% yield of MPAN from methacrolein. Briefly, the biogenic source of MPAN, even in the Colorado Front Range, is still at least an order of magnitude larger than a potential anthropogenic source.

3.4. PANs and Ozone

PAN is considered to be strong indicator of photochemical activity or long-range transport of polluted air parcels because PAN is not emitted directly, and relative to O_3, it has a low background. Similar to other regions (e.g., Roberts et al., 1995), we observed a positive relationship between O_3 and PAN at BAO during summer 2014 ($R^2 = 0.42$ for all hourly averaged data between 10 a.m. and 6 p.m.). Due to the electrical noise discussed in section 2.2, we have the most complete PAN data set at BAO in July. Figure 6 shows that during this window there were five days where hourly average O_3 mixing ratios greatly exceeded 80 ppbv at BAO (19, 22, 23, 28, and 29 July). PAN was also elevated (hourly average mixing ratios exceeded the 90th percentile for the entire data set for 10 a.m. to 6 p.m.) on four of the five days.

Figure 6 presents the relationships between PPN, MPAN, and PAN on the five days with the most elevated O_3 at BAO during 2014. Four of the days have PPN/PAN ratios greater than 0.15. The conditions associated with the high O_3 on 19 July appear to be different than the other days. PAN mixing ratios were lower at BAO on this day, only reaching ~400 pptv (Figure 6c), and the PPN to PAN ratio was lower (Figure 6a). This is in contrast to the other dates with elevated O_3 during July. Regional winds (NWS sites) showed a consistent downslope wind until about 10 LT on 19 July, and air parcel loading plots (similar to those presented in Figure 2) show that BAO was influenced by emissions located to the west. There was a timing disconnect between the hourly maximum O_3 (16:00 MT) and the hourly maximum PAN (13:00 MT). There were no PAN or O_3 data at RMNP on this day because the air conditioners in the instrument trailer had failed. Model simulations conducted during the field campaign indicate that both long-range transport of wildfire smoke and stratosphere-troposphere exchange may have contributed to the elevated surface ozone on 19 July.
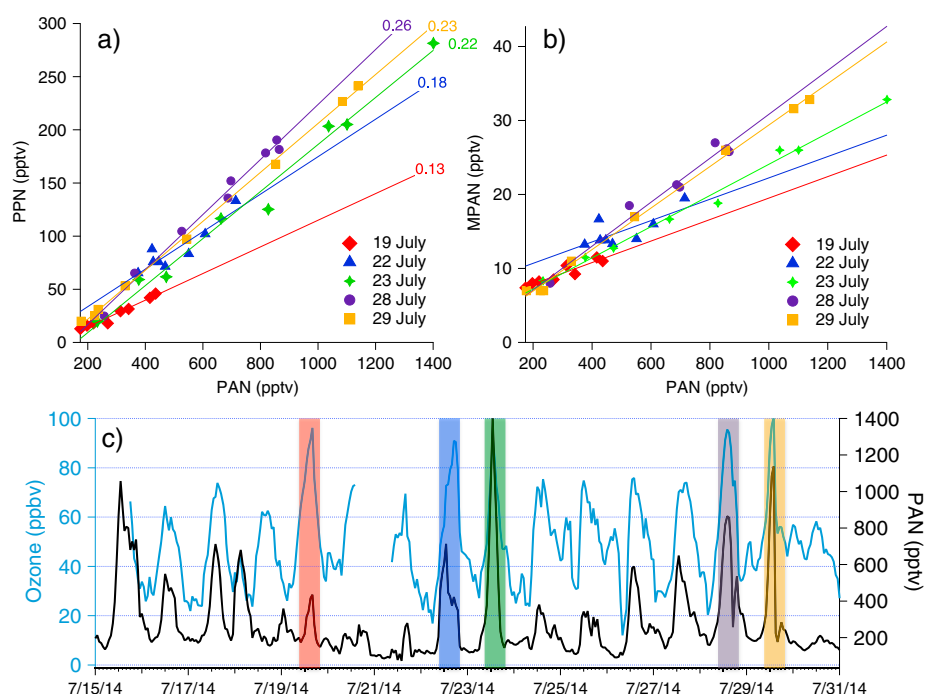
Figure 6. (a) 10:00–18:00 MT hourly average PPN versus PAN at BAO for 5 days in July 2014. The numbers indicate the slope of each subset of data. This information is also presented in Table 2. (b) The 10:00–18:00 MT hourly average MPAN versus PAN for 5 days in July 2014. (c) Time series of hourly average PAN and O_3 at BAO between 15 and 31 July 2014 with five elevated O_3 periods highlighted using the same color scheme as Figures 6a and 6b.

The hourly maximum O_3 and PAN occurred at the same time on 23, 28, and 29 July, but there was an earlier hourly maximum PAN peak on 22 July (13:00 MT) versus O_3 (17:00 MT). Three Front Range O_3 monitoring sites, Rocky Flats North, National Renewable Energy Laboratory, and Fort Collins-West each violated the 2008 NAAQS on 22 July (Sullivan et al., 2016). Sullivan et al. (2016) show that a mountain-plain solenoid circulation was established on this day and that the recirculation of polluted return flow aloft exacerbated surface O_3 across the region. As described in Sullivan et al. (2016), mountain-plain solenoid circulation in the Front Range is characterized by upslope flow near the surface, rising motion near the Rocky Mountains, westerly flow aloft, and sinking motion over the Colorado plains. Sullivan et al. (2016) report similar late afternoon (15:00–17:00 MT) increases in O_3 at the monitoring sites. Based on the lidar data, background O_3 on this day was 51 ppbv, lower than the campaign average of 57 ppbv (McDuffie et al., 2016). Figure 2 shows that RMNP PAN mixing ratios exceeded those at BAO on 22 July, reaching 1,345 pptv. Clear increases in O_3 and a suite of VOCs were also observed during this time at RMNP (Callahan et al., 2014). Further details on this event will be the topic of a subsequent manuscript.

MPAN measured during FRAPPÉ had a mean mixing ratio of 9 pptv with a maximum of 36 pptv (see Table 1). Figure 6b presents the relationship between MPAN and PAN on the five days discussed above. The slopes associated with the linear fits are provided in Table 2. Four of the five days with elevated O_3 presented MPAN to PAN ratios ranging from 0.04 to 0.02. Both the relative and the absolute MPAN abundances are very small compared to those measured during previous campaigns in the eastern and southern U.S. For example, mean and maximum values of 27 and 371 pptv were observed during the 2002 New England Air Quality Study (Roberts et al., 2007), mean and maximum values of 15 and 210 pptv were observed during the 2000 Texas Air Quality Study (Roberts et al., 2003), and mean and maximum values of 30 and 150 pptv were observed during the 1995 Southern Oxidant Study (Nouaime et al.,
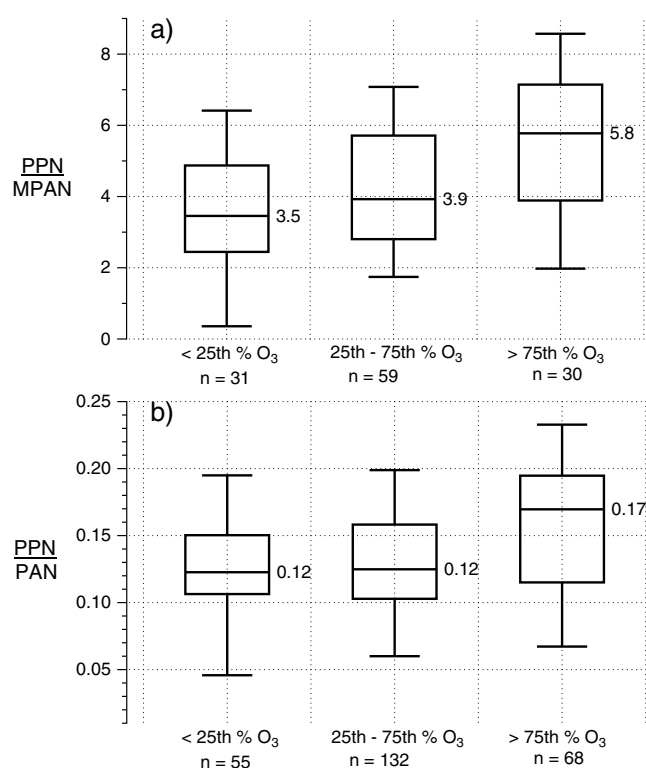
Table 2
Relationships Between APNs at BAO Between 10:00 and 18:00 MT on Selected Days During July 2014

| Date | PPN Versus PAN | | MPAN Versus PAN | | Background O_3 (ppbv) |
	R^2	Slope	R^2	Slope	
19 July	0.97	0.13	0.89	0.015	58
22 July	0.83	0.18	0.56	0.014	51
23 July	0.98	0.22	0.99	0.021	53
28 July	0.99	0.26	0.97	0.030	67
29 July	1.0	0.23	1.0	0.028	68

Figure 7. (a) Distribution of PPN:MPAN ratios at BAO using hourly average points between 10:00 and 18:00 MT for three subsets of hourly O_3 values (<25th percentile, 25th–75th percentiles, and >75th percentile), and (b) distribution of PPN:PAN ratios at BAO using hourly average points between 10:00 and 18:00 MT for three subsets of hourly O_3 values (<25th percentile, 25th–75th percentiles, and >75th percentile). The boxes enclose the 25th to 75th percentiles; the whiskers represent the 5th and 95th percentiles. The medians are labeled. Note that there are different numbers of points included in panel because MPAN data are only available for the first portion of the campaign due to electrical noise.

1998). Williams et al. (1997) reported MPAN to PAN ratios on the order of 0.1; MPAN is one half to one quarter as abundant relative to PAN in the Front Range as compared to observations in the Southeast.

Williams et al. (1997) used relative abundances of measured PAN, PPN, and MPAN during the 1995 Southern Oxidant Study with a linear model to estimate the contribution of isoprene chemistry to O_3 production. We examined the utility of this approach applied to the five days with the highest O_3 at the BAO tower during FRAPPÉ However, this model cannot provide a meaningful estimate of the contribution of biogenic versus anthropogenic VOCs in the Front Range air basin because the signal from isoprene chemistry, in the form of MPAN, is simply too weak. This is very different from the Williams et al. (1997) data set collected in an isoprene-rich region of the eastern U.S. For example, the degrees of correlation between measured PPN and PAN and measured MPAN and PAN were much lower than we observed, $r^2 = 0.27$ and $r^2 = 0.57$, respectively.

The analysis of McDuffie et al. (2016) also indicates that the use of a single value for background O_3 applied to individual days is inappropriate for our region. Derived from O_x/NO_z correlation plots for 15 min data intervals throughout FRAPPÉ, McDuffie et al. (2016) report an average background O_3 of 56.7 ppbv but with a large, 1σ range of 9.3 ppbv. Daily background O_3 mixing ratios can additionally be derived from lidar measurements (e.g., McDuffie et al., 2016) using average O_3 at 500 m and at 2 km between 8:00 and 11:00 MT. Our use of the word background refers to the O_3 present at the start of photochemical production on a given day; it does *not* refer to O_3 present without local anthropogenic emissions. Lidar data were available on 22, 23, 28, and 29 July and provide daily O_3 background mixing ratios that range from 51 to 68 ppbv (Table 2). On 19 July, the lidar was not running and NO_x data were only available until 11:00 MT. The average intercept from the 8:00–11:00 MT O_x/NO_z correlation plots for that period was 58 ppbv, so we consider the best available estimate of background O_3 on 19 July for BAO. Table 2 shows that there are weaker individual relationships between MPAN and PAN ($R^2 = 0.53$) and PPN and PAN ($R^2 = 0.83$) on 22 July. However, following the approach of Williams et al. (1997) to calculate the mixing ratio of PAN as a linear combination of observed MPAN and PPN abundances between 10:00 and 18:00 MT on 22 July yields an unrealistic (i.e., negative coefficient) contribution from MPAN. MPAN has a shorter lifetime against thermal decomposition compared to PAN or PPN; if recirculation played an important role on this day, differential loss of MPAN relative to PAN and PPN may be the reason that the linear combination approach yields unrealistic results.

Figure 7 presents a summary of the ratio of PPN to MPAN and PPN to PAN abundances at BAO during FRAPPÉ between 10:00 and 18:00 MT for low (<25th percentile), medium (25th–75th percentiles), and high (>75th percentile) hourly average O_3 mixing ratios. Figure 7a implies that the importance of isoprene for PAN production, and thus likely O_3 production, generally decreases with increasing O_3. Figure 7b shows that hourly average O_3 mixing ratios at BAO >75th percentile coincide with higher median PPN to PAN ratios. Figure 8 presents the relationship between O_3 and the ratio of PPN to PAN observed from the C-130 during FRAPPÉ. Figure 8a shows that O_3 >75th percentile (71.5 ppbv for the 60 s average) is much more likely to be associated with PPN to PAN ratios >0.15 and O_3 >95th percentile (81.6 ppbv for the 60 s average) is only associated with PPN to PAN ratios >0.15. Figure 8 also shows that PPN to PAN ratios notably higher than 0.15 were observed from the C-130 during FRAPPÉ, and these air parcels were not associated with O_3 >95th percentile. These points were associated with relatively cool temperatures for afternoon samples (Figure 8b) and were largely associated with a single flight on 31 July 2014 (Julian Day 212). Ratios of PPN to PAN significantly higher than 0.15, such as those observed by the C-130 on 31 July 2014, have also
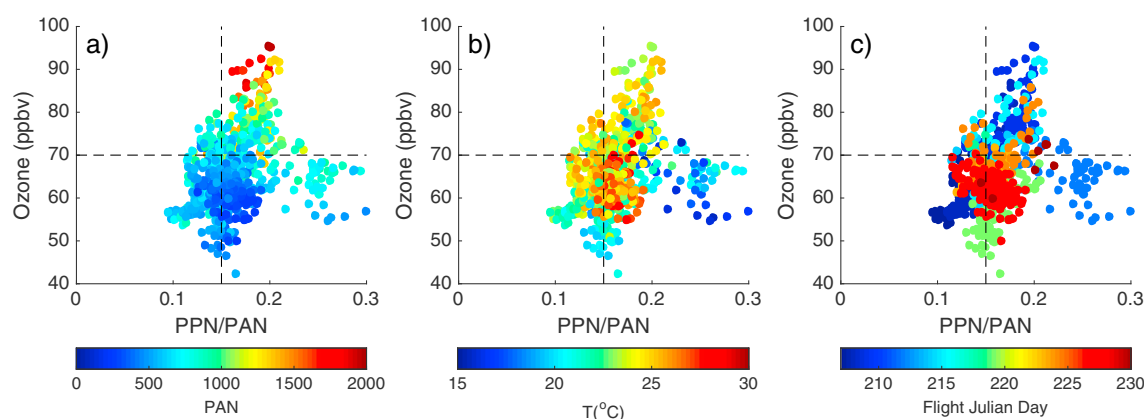
Figure 8. O_3 versus the coincident PPN:PAN ratio observed from the C-130 aircraft in the boundary layer (<2.5 km above mean ground level, 12–18 MT) over the Colorado Front Range (38.5–41.0°N, 105.3–103°W colored by (a) PAN, (b) temperature, and (c) flight Julian day. These plots use data from the 60 s merge. The dashed horizontal lines indicate the 75th and 95th percentiles of this subset of data. The dashed vertical line is set at a PPN/PAN ratio of 0.15, a ratio that has been observed in areas dominated by anthropogenic VOC-NO$_x$ photochemistry.

been observed (1) in Houston when the VOC precursor mixture was strongly impacted by local petrochemical sources (Roberts et al., 2003), (2) near California in the marine boundary layer where thermal decomposition likely substantially reduced the lifetime of PAN relative to PPN (Roberts et al., 2004), and over New England within a heavily polluted and photochemically aged air parcel (Roberts et al., 2007). The PAN chemistry observed at BAO and from the C-130 during FRAPPÉ implies that anthropogenic VOCs played a dominant role in PAN production during periods with the most O_3 and that the relative importance of isoprene in photochemical O_3 production generally decreased with increasing O_3 during FRAPPÉ.

4. Summary

The PAN chemistry observed during FRAPPÉ implies that anthropogenic VOCs played a dominant role in PAN production during periods with the most local O_3 production. The following bullets provide support for this conclusion:

1. The highest PAN mixing ratios observed at BAO during summer 2014 were consistently associated with high PPN/PAN ratios (>0.15). A PPN/PAN ratio of 0.15 has been observed in other regions where PAN production is driven by a mixture of anthropogenic VOCs. In the Colorado Front Range, the highest PAN mixing ratios do not show large variability, reflecting little variability in anthropogenically dominated VOC chemistry on the most polluted days. The RMA slope of 0.21 for PPN versus PAN was heavily weighted by the highest PAN and PPN mixing ratios, and we hypothesize that this relatively high PPN/PAN ratio is the result of a VOC mixture that contains a higher abundance of alkanes from oil and gas production compared to other U.S. urban regions.

2. The MPAN abundances observed at BAO during July 2014 were very small compared to those measured during previous campaigns in the eastern and southern U.S. Thus, the signal of O_3 production from isoprene chemistry during July 2014 is very weak.

3. Of the days in July 2014 with hourly average O_3 mixing ratios greater than 80 ppbv, there was one day (19 July) where the presence of elevated O_3 (hourly average mixing ratios >80 ppbv) appears to be disconnected from local PAN production. The contribution of isoprene oxidation to PAN production on the other days in July with elevated O_3 (22, 23, 28, and 29 July) appears to be small. PPN to PAN ratios coincident with the most elevated O_3 were all above 0.15, indicating that PAN and O_3 production on the most polluted days was largely driven by anthropogenic VOC sources.

4. The PPN/MPAN ratio and the PPN/PAN ratio increased with increasing O_3 during FRAPPÉ based on observations from the BAO tower. Ozone observed above the 95th percentile in the boundary layer from the C-130 research aircraft during FRAPPÉ was also consistently associated with PPN/PAN ratios above 0.15. Thus, it appears that the role of biogenic VOCs in O_3 production in the Front Range is minimal when O_3 is highest.

References

Abeleira, A., Pollack, I. B., Sive, B., Zhou, Y., Fischer, E. V., & Farmer, D. K. (2017). Source characterization of volatile organic compounds in the Colorado Northern Front Range Metropolitan Area during spring and summer 2015. *Journal of Geophysical Research: Atmospheres*, *122*. https://doi.org/10.1002/2016JD026227

Abeleira, A. A., & Farmer, D. K. (2017). Summer ozone in the Northern Front Range Metropolitan Area: Weekend-weekday effects, temperature dependences and the impact of drought. *Atmospheric Chemistry and Physics*, *17*(11), 6517–6529, https://doi.org/10.5194/acp-17-6517-2017

Atkinson, R., Tuazon, E. C., & Carter, W. P. L. (1985). Extent of H-atom abstraction from the reaction of the OH radical with 1-butene under atmospheric conditions. *International Journal of Chemical Kinetics*, *17*(7), 725–734. https://doi.org/10.1002/kin.550170703

Benedict, K. B., Carrico, C. M., Kreidenweis, S. M., Schichtel, B., Malm, W. C., & Collett, J. L. (2013). A seasonal nitrogen deposition budget for Rocky Mountain National Park. *Ecological Applications*, *23*(5), 1156–1169, 1890/12-1624.1. https://doi.org/10.1890/12-1624.1

Bertman, S. B., & Roberts, J. M. (1991). A PAN analog from isoprene photooxidation. *Geophysical Research Letters*, *18*(8), 1461–1464. https://doi.org/10.1029/91GL01852

Biesenthal, T. A., & Shepson, P. B. (1997). Observations of anthropogenic inputs of the isoprene oxidation products methyl vinyl ketone and methacrolein to the atmosphere. *Geophysical Research Letters*, *24*(11), 1375–1378. https://doi.org/10.1029/97GL01337

Brioude, J., Arnold, D., Stohl, A., Cassiani, M., Morton, D., Seibert, P., … Wotawa, G. (2013). The Lagrangian particle dispersion model FLEXPART-WRF version 3.1. *Geoscientific Model Development*, *6*(6), 1889–1904. https://doi.org/10.5194/gmd-6-1889-2013

Brophy, P., & Farmer, D. K. (2015). A switchable reagent ion high resolution time-of-flight chemical ionization mass spectrometer for real-time measurement of gas phase oxidized species: Characterization from the 2013 southern oxidant and aerosol study. *Atmospheric Measurement Techniques*, *8*(7), 2945–2959. https://doi.org/10.5194/amt-8-2945-2015

Brown, S. S., Thornton, J. A., Keene, W. C., Pszenny, A. A. P., Sive, B. C., Dubé, W. P., … Wolfe, D. E. (2013). Nitrogen, Aerosol Composition, and Halogens on a Tall Tower (NACHTT): Overview of a wintertime air chemistry field study in the front range urban corridor of Colorado. *Journal of Geophysical Research: Atmospheres*, *118*, 8067–8085. https://doi.org/10.1002/jgrd.50537

Callahan, S. L., Fischer, E. V., Zhou, Y., & Sive, B. C. (2014). PAN among the peaks: A preliminary analysis of new peroxyacetyl nitrate (PAN) measurements in Rocky Mountain National Park, American Geophysical Union Annual Meeting, Abstract A13E-3219.

Cooper, O. R., Langford, A. O., Parrish, D. D., & Fahey, D. W. (2015). Challenges of a lowered U.S. ozone standard. *Science*, *348*(6239), 1096–1097. https://doi.org/10.1126/science.aaa5748

Cooper, O. R., Parrish, D. D., Ziemke, J., Balashov, N. V., Cupeiro, M., Galbally, I. E., … Zbinden, R. M. (2014). Global distribution and trends of tropospheric ozone: An observation-based review. *Elementa: Science of the Anthropocene*, *2*. https://doi.org/10.12952/journal.elementa.000029

Dingle, J. H., Vu, K., Bahreini, R., Apel, E. C., Campos, T. L., Flocke, F., … Weinheimer, A. (2016). Aerosol optical extinction during the Front Range Air Pollution and Photochemistry Éxperiment (FRAPPÉ) 2014 summertime field campaign, Colorado, USA. *Atmospheric Chemistry and Physics*, *16*(17), 11,207–11,217. https://doi.org/10.5194/acp-16-11207-2016

Droege, A. T., & Tully, F. P. (1986). Hydrogen-atom abstraction from alkanes by hydroxyl. 3. Propane. *Journal of Physical Chemistry*, *90*(9), 1949–1954. https://doi.org/10.1021/j100400a042

Ellis, R. A., Murphy, J. G., Pattey, E., van Haarlem, R., O'Brien, J. M., & Herndon, S. C. (2010). Characterizing a quantum cascade tunable infrared laser differential absorption spectrometer (QC-TILDAS) for measurements of atmospheric ammonia. *Atmospheric Measurement Techniques*, *3*(2), 397–406. https://doi.org/10.5194/amt-3-397-2010

Fischer, E. V., Jacob, D. J., Yantosca, R. M., Sulprizio, M. P., Millet, D. B., Mao, J., … Deolal, S. P. (2014). Atmospheric peroxyacetyl nitrate (PAN): A global budget and source attribution. *Atmospheric Chemistry and Physics*, *14*(5), 2679–2698. https://doi.org/10.5194/acp-14-2679-2014

Flocke, F., Weinheimer, A., Swanson, A., Roberts, J., Schmitt, R., & Shertz, S. (2005). On the measurement of PANs by gas chromatography and electron capture detection. *Journal of Atmospheric Chemistry*, *52*(1), 19–43. https://doi.org/10.1007/s10874-005-6772-0

Gilman, J. B., Lerner, B. M., Kuster, W. C., & de Gouw, J. A. (2013). Source signature of volatile organic compounds from oil and natural gas operations in northeastern Colorado. *Environmental Science & Technology*, *47*(3), 1297–1305. https://doi.org/10.1021/es304119a

Grosjean, E., Grosjean, D., & Woodhouse, L. F. (2001). Peroxyacetyl nitrate and peroxypropionyl nitrate during SCOS 97-NARSTO. *Environmental Science & Technology*, *35*(20), 4007–4014. https://doi.org/10.1021/es010640h

Guenther, A., Karl, T., Harley, P., Wiedinmyer, C., Palmer, P. I., & Geron, C. (2006). Estimates of global terrestrial isoprene emissions using MEGAN (Model of Emissions of Gases and Aerosols from Nature). *Atmospheric Chemistry and Physics*, *6*(11), 3181–3210. https://doi.org/10.5194/acp-6-3181-2006

Hahn, C. (1981). A study of the diurnal behavior of boundary-layer winds at the Boulder Atmospheric Observatory. *Boundary-Layer Meteorology*, *21*(2), 231–245. https://doi.org/10.1007/BF02033941

Helmig, D., Thompson, C. R., Evans, J., Boylan, P., Hueber, J., & Park, J. H. (2014). Highly elevated atmospheric levels of volatile organic compounds in the Uintah Basin, Utah. *Environmental Science & Technology*, *48*(9), 4707–4715. https://doi.org/10.1021/es405046r

Jonsson, A., Persson, K. A., & Grigoriadis, V. (1985). Measurements of some low molecular-weight oxygenated, aromatic, and chlorinated hydrocarbons in ambient air and in vehicle emissions. *Environment International*, *11*(2-4), 383–392. https://doi.org/10.1016/0160-4120(85)90033-9

Kaimal, J. C., & Gaynor, J. E. (1983). The Boulder Atmospheric Observatory. *Journal of Climate and Applied Meteorology*, *22*(5), 863–880. https://doi.org/10.1175/1520-0450(1983)022%3C0863:TBAO%3E2.0.CO;2

McDuffie, E. E., Edwards, P. M., Gilman, J. B., Lerner, B. M., Dubé, W. P., Trainer, M., … Brown, S. S. (2016). Influence of oil and gas emissions on summertime ozone in the Colorado Northern Front Range. *Journal of Geophysical Research: Atmospheres*, *121*, 8712–8729. https://doi.org/10.1002/2016JD025265

McLaren, R., Singleton, D. L., Lai, J. Y. K., Khouw, B., Singer, E., Wu, Z., & Niki, H. (1996). Analysis of motor vehicle sources and their contribution to ambient hydrocarbon distributions at urban sites in Toronto during the Southern Ontario oxidants study. *Atmospheric Environment*, *30*(12), 2219–2232. https://doi.org/10.1016/1352-2310(95)00178-6

Millet, D. B., Baasandorj, M., Farmer, D. K., Thornton, J. A., Baumann, K., Brophy, P., … Xu, J. (2015). A large and ubiquitous source of atmospheric formic acid. *Atmospheric Chemistry and Physics*, *15*(11), 6283–6304. https://doi.org/10.5194/acp-15-6283-2015

Nouaime, G., Bertman, S. B., Seaver, C., Elyea, D., Huang, H., Shepson, P. B., … Olszyna, K. (1998). Sequential oxidation products from tropospheric isoprene chemistry: MACR and MPAN at a NO x -rich forest environment in the southeastern United States. *Journal of Geophysical Research*, *103*(D17), 22,463–22,471. https://doi.org/10.1029/98JD00320

Pétron, G., Frost, G., Miller, B. R., Hirsch, A. I., Montzka, S. A., Karion, A., … Tans, P. (2012). Hydrocarbon emissions characterization in the Colorado Front Range: A pilot study. *Journal of Geophysical Research*, *117*, D04304. https://doi.org/10.1029/2011JD016360

Pétron, G., Karion, A., Sweeney, C., Miller, B. R., Montzka, S. A., Frost, G. J., … Schnell, R. (2014). A new look at methane and nonmethane hydrocarbon emissions from oil and natural gas operations in the Colorado Denver-Julesburg Basin. *Journal of Geophysical Research: Atmospheres*, *119*, 6836–6852. https://doi.org/10.1002/2013JD021272

Reddy, P. J., & Pfister, G. G. (2016). Meteorological factors contributing to the interannual variability of midsummer surface ozone in Colorado, Utah, and other western U.S. states. *Journal of Geophysical Research: Atmospheres*, *121*, 2434–2456. https://doi.org/10.1002/2015JD023840

Ridley, B. A., Shetter, J. D., Walega, J. G., Madronich, S., Elsworth, C. M., Grahek, F. E., … Westberg, H. H. (1990). The behavior of some organic nitrates at Boulder and Niwot Ridge, Colorado. *Journal of Geophysical Research*, *95*(D9), 13,949–13,961. https://doi.org/10.1029/JD095iD09p13949

Roberts, J. M., Flocke, F., Chen, G., de Gouw, J., Holloway, J. S., Hübler, G., … Fehsenfeld, F. C. (2004). Measurement of peroxycarboxylic nitric anhydrides (PANs) during the ITCT 2K2 aircraft intensive experiment. *Journal of Geophysical Research*, *109*, D23S21. https://doi.org/10.1029/2004JD004960

Roberts, J. M., Flocke, F., Stroud, C. A., Hereid, D., Williams, E. J., Fehsenfeld, F. C., … Harder, H. (2002). Ground-based measurements of PANs during the 1999 Southern Oxidants Study Nashville intensive. *Journal of Geophysical Research*, *107*, 4554. https://doi.org/10.1029/2001JD000947

Roberts, J. M., Jobson, B. T., Kuster, W., Goldan, P., Murphy, P., Williams, E., … Fehsenfeld, F. (2003). An examination of the chemistry of peroxycarboxylic nitric anhydrides and related volatile organic compounds during Texas Air Quality Study 2000 using ground-based measurements. *Journal of Geophysical Research*, *108*, ACH 4-1, ACH 4-12. https://doi.org/10.1029/2003JD003383

Roberts, J. M., Marchewka, M., Bertman, S. B., Sommariva, R., Warneke, C., de Gouw, J., … Fehsenfeld, F. C. (2007). Measurements of PANs during the New England Air Quality Study 2002. *Journal of Geophysical Research*, *112*, D20306. https://doi.org/10.1029/2007JD008667

Roberts, J. M., Stroud, C. A., Jobson, B. T., Trainer, M., Hereid, D., Williams, E., … Harder, H. (2001). Application of a sequential reaction model to PANs and aldehyde measurements in two urban areas. *Geophysical Research Letters*, *28*(24), 4583–4586. https://doi.org/10.1029/2001GL013507

Roberts, J. M., Tanner, R. L., Newman, L., Bowersox, V. C., Bottenheim, J. W., Anlauf, K. G., … Bailey, E. M. (1995). Relationships between PAN and ozone at sites in eastern North America. *Journal of Geophysical Research*, *100*(D11), 22,821–22,830. https://doi.org/10.1029/95JD01221

Roberts, J. M., Williams, J., Baumann, K., Buhr, M. P., Goldan, P. D., Holloway, J., … Young, V. L. (1998). Measurements of PAN, PPN, and MPAN made during the 1994 and 1995 Nashville Intensives of the Southern Oxidant Study: Implications for regional ozone production from biogenic hydrocarbons. *Journal of Geophysical Research*, *103*(D17), 22,473–22,490. https://doi.org/10.1029/98JD01637

Schauer, J. J., Kleeman, M. J., Cass, G. R., & Simoneit, B. R. T. (2002). Measurement of emissions from air pollution sources. 5. C1−C32 organic compounds from gasoline-powered motor vehicles. *Environmental Science & Technology*, *36*(6), 1169–1180. https://doi.org/10.1021/es0108077

Sillman, S., & Samson, P. J. (1995). Impact of temperature on oxidant photochemistry in urban, polluted rural and remote environments. *Journal of Geophysical Research*, *100*(D6), 11,497–11,508. https://doi.org/10.1029/94JD02146

Simon, H., Reff, A., Wells, B., Xing, J., & Frank, N. (2015). Ozone trends across the United States over a period of decreasing NO$_x$ and VOC emissions. *Environmental Science & Technology*, *49*(1), 186–195. https://doi.org/10.1021/es504514z

Singh, H. B. (1987). Reactive nitrogen in the troposphere. *Environmental Science & Technology*, *21*(4), 320–327. https://doi.org/10.1021/es00158a001

Singh, H. B., & Hanst, P. L. (1981). Peroxyacetyl nitrate (PAN) in the unpolluted atmosphere: An important reservoir for nitrogen oxides. *Geophysical Research Letters*, *8*(8), 941–944. https://doi.org/10.1029/GL008i008p00941

Singh, H. B., Herlth, D., O'Hara, D., Zahnle, K., Bradshaw, J. D., Sandholm, S. T., … Wofsy, S. C. (1994). Summertime distribution of PAN and other reactive nitrogen species in the northern high-latitude atmosphere of eastern Canada. *Journal of Geophysical Research*, *99*(D1), 1821–1835. https://doi.org/10.1029/93JD00946

Singh, H. B., Salas, L. J., Ridley, B. A., Shetter, J. D., Donahue, N. M., Fehsenfeld, F. C., … Murphy, P. C. (1985). Relationship between peroxyacetyl nitrate and nitrogen oxides in the clean troposphere. *Nature*, *318*(6044), 347–349. https://doi.org/10.1038/318347a0

Stohl, A., Forster, C., Frank, A., Seibert, P., & Wotawa, G. (2005). Technical note: The Lagrangian particle dispersion model FLEXPART version 6.2. *Atmospheric Chemistry and Physics*, *5*(9), 2461–2474. https://doi.org/10.5194/acp-5-2461-2005

Strode, S. A., Rodriguez, J. M., Logan, J. A., Cooper, O. R., Witte, J. C., Lamsal, L. N., … Strahan, S. E. (2015). Trends and variability in surface ozone over the United States. *Journal of Geophysical Research: Atmospheres*, *120*, 9020–9042. https://doi.org/10.1002/2014JD022784

Sullivan, J. T., McGee, T. J., Langford, A. O., Alvarez, R. J., Senff, C. J., Reddy, P. J., … Hoff, R. M. (2016). Quantifying the contribution of thermally driven recirculation to a high-ozone event along the Colorado Front Range using lidar. *Journal of Geophysical Research: Atmospheres*, *121*, 10,377–10,390. https://doi.org/10.1002/2016JD025229

Swarthout, R. F., Russo, R. S., Zhou, Y., Hart, A. H., & Sive, B. C. (2013). Volatile organic compound distributions during the NACHTT campaign at the Boulder Atmospheric Observatory: Influence of urban and natural gas sources. *Journal of Geophysical Research: Atmospheres*, *118*, 10,614–10,637. https://doi.org/10.1002/jgrd.50722

Taylor, O. C. (1969). Importance of peroxyacetyl nitrate (PAN) as a phytotoxic air pollutant. *Journal of the Air Pollution Control Association*, *19*(5), 347–351. https://doi.org/10.1080/00022470.1969.10466498

Tevlin, A. G., Li, Y., Collett, J. L., McDuffie, E. E., Fischer, E. V., & Murphy, J. G. (2017). Tall tower vertical profiles and diurnal trends of ammonia in the Colorado Front Range. *Journal of Geophysical Research: Atmospheres*, *122*. https://doi.org/10.1002/2017JD026534

Thompson, C., Hueber, J., & Helmig, D. (2014). Influence of oil and gas emissions on ambient atmospheric non-methane hydrocarbons in residential areas of Northeastern Colorado. *Elementa Science of the Anthropocene*, *2*. https://doi.org/10.12952/journal.elementa.000035

Townsend-Small, A., Botner, E. C., Jimenez, K. L., Schroeder, J. R., Blake, N. J., Meinardi, S., … Flocke, F. M. (2016). Using stable isotopes of hydrogen to quantify biogenic and thermogenic atmospheric methane sources: A case study from the Colorado Front Range. *Geophysical Research Letters*, *43*(21), 11,462–11,471. https://doi.org/10.1002/2016GL071438

Tuazon, E. C., & Atkinson, R. (1990). A product study of the gas-phase reaction of Methacrolein with the OH radical in the presence of NO$_x$. *International Journal of Chemical Kinetics*, *22*(6), 591–602. https://doi.org/10.1002/kin.550220604

Volz-Thomas, A., Xueref, I., & Schmitt, R. (2002). Automatic gas chromatograph and calibration system for ambient measurements of PAN and PPN. *Environmental Science and Pollution Research*, *9*, 72–76.

Vu, K. T., Dingle, J. H., Bahreini, R., Reddy, P. J., Apel, E. C., Campos, T. L., … Flocke, F. (2016). Impacts of the Denver cyclone on regional air quality and aerosol formation in the Colorado Front Range during FRAPPÉ 2014. *Atmospheric Chemistry and Physics*, *16*(18), 12,039–12,058. https://doi.org/10.5194/acp-16-12039-2016

Vyskocil, A., Viau, C., & Lamy, S. (1998). Peroxyacetyl nitrate: Review of toxicity. *Human & Experimental Toxicology*, *17*(4), 212–220. https://doi.org/10.1177/096032719801700403

Warneck, P., & Zerbach, T. (1992). Synthesis of peroxyacetyl nitrate in air by acetone photolysis. *Environmental Science & Technology*, *26*(1), 74–79. https://doi.org/10.1021/es00025a005

Warneke, C., Geiger, F., Edwards, P. M., Dube, W., Pétron, G., Kofler, J., … Roberts, J. M. (2014). Volatile organic compound emissions from the oil and natural gas industry in the Uintah Basin, Utah: Oil and gas well pad emissions compared to ambient air composition. *Atmospheric Chemistry and Physics*, *14*(20), 10,977–10,988. https://doi.org/10.5194/acp-14-10977-2014

Wiedinmyer, C., Akagi, S. K., Yokelson, R. J., Emmons, L. K., Al-Saadi, J. A., Orlando, J. J., & Soja, A. J. (2011). The Fire INventory from NCAR (FINN): A high resolution global model to estimate the emissions from open burning. *Geoscientific Model Development*, *4*(3), 625–641. https://doi.org/10.5194/gmd-4-625-2011

Williams, J., Roberts, J. M., Fehsenfeld, F. C., Bertman, S. B., Buhr, M. P., Goldan, P. D., … Young, V. (1997). Regional ozone from biogenic hydrocarbons deduced from airborne measurements of PAN, PPN, and MPAN. *Geophysical Research Letters*, *24*(9), 1099–1102. https://doi.org/10.1029/97GL00548

Zaragoza, J. (2016). *Observations of acyl peroxy nitrates during the Front Range Air Pollution and Photochemistry Experiement (FRAPPÉ)* (p. 72). Fort Collins, CO: Colorado State University.

Zheng, W., Flocke, F. M., Tyndall, G. S., Swanson, A., Orlando, J. J., Roberts, J. M., … Tanner, D. J. (2011). Characterization of a thermal decomposition chemical ionization mass spectrometer for the measurement of peroxy acyl nitrates (PANs) in the atmosphere. *Atmospheric Chemistry and Physics*, *11*(13), 6529–6547. https://doi.org/10.5194/acp-11-6529-2011